Planetary and Space Science 126 (2016) 78–92

Contents lists available at ScienceDirect

Planetary and Space Science

journal homepage: www.elsevier.com/locate/pss

Jupiter spin-pole precession rate and moment of inertia from Juno radio-science observations

S. Le Maistre [a,*], W.M. Folkner [a], R.A. Jacobson [a], D. Serra [b]

[a] Jet Propulsion Laboratory, California Institute of Technology, 4800 Oak Grove Dr, Pasadena, CA 91109, USA
[b] Department of Mathematics, University of Pisa, I-56127 Pisa, Italy

ARTICLE INFO

Article history:
Received 20 October 2015
Accepted 11 March 2016
Available online 18 March 2016

Keywords:
Jupiter
Interior
Orientation
Orbit determination
Radio-science
Numerical simulations

ABSTRACT

Through detailed and realistic numerical simulations, the present paper assesses the precision with which the Juno spacecraft can measure the normalized polar moment of inertia (MOI) of Jupiter. Based on Ka-band Earth-based Doppler data, created with realistic 10 μm/s of white noise at 60 s of integration, this analysis shows that the determination of the precession rate of Jupiter is by far more efficient than the Lense–Thirring effect previously proposed to determine the moment of inertia and therefore to constrain the internal structure of the giant planet with Juno.

We show that the Juno mission will allow the estimation of the precession rate of Jupiter's pole with an accuracy better than 0.1%. We provide an equation relating the pole precession rate and the normalized polar moment of inertia of Jupiter. Accounting for the uncertainty in the parameters affecting precession, we show that the accuracy of the MOI inferred from the precession rate is also better than 0.1%, and at least 50 times better than inferred from the Lense–Thirring acceleration undergone by Juno. This accuracy of the MOI determination should provide tight constraints on the interior structure of Jupiter, especially the core size and mass, helping to distinguish among competing scenarios of formation and evolution of the giant planet.

In addition, though the Juno mission operations are already defined, the exact duration of the tracking and its occurrence with respect to the spacecraft pericenter pass are not definitely scheduled. The simulations performed here quantify the impact of this aspect of the mission on the Juno sensitivity to (in particular) the spin-pole precession rate of Jupiter.

Finally, additional simulations have been performed to test the usefulness of combining Doppler data with VLBI data, showing the latter measurements to be 10^4–10^5 times less sensitive than the former to our parameters of interest and therefore, obviously, totally needless.

1. Introduction

The Juno New Frontiers NASA mission was launched on August 5, 2011 and is now en route to Jupiter. After a five-year trip, the spacecraft will be injected on July 5, 2016 into an highly elliptical 53-day polar orbit around the giant planet. After two revolutions, Juno's orbital period will be reduced to 14 days for science operation. The spacecraft will orbit Jupiter 36 times over 595 days before deorbit into its atmosphere. The mission aims to study the planet's composition and interior structure, gravity field, magnetic field, and polar magnetosphere in order to investigate the origin and evolution of the giant planet (Matousek, 2007; Bolton, 2010).

Among nine scientific instruments, the payload of Juno includes radio-science instruments that will be used to accurately map the gravity field of Jupiter through classical Precise Orbit Determination (POD) techniques (e.g. Iess et al., 2013; Tommei et al., 2015). In addition to the gravity field, the very accurate reconstruction of the orbit of Juno enabled by the high precision Ka-band Doppler data will permit, among others, the determination of the main moments of inertia (MOI) of the giant planet. MOI characterize the internal mass distribution inside the planet. Such information about the interior structure is key for the understanding of the planet's formation and evolution (Guillot and Gautier, 2007).

The MOI of Jupiter can be inferred (1) from the degree-two gravity coefficient assuming the planet to be at the hydrostatic equilibrium, (2) from the planet orientation changing (precession) and (3) from the Lense–Thirring relativistic acceleration experienced by the spacecraft (Iorio, 2010; Helled et al., 2011). Expected to be very small, the acceleration experienced by Juno due to Jupiter pole precession rate has not been analyzed in detail before. So far, only Helled et al. (2011) considered Jupiter's polar

* Corresponding author. Tel.: +1 818 354 4381.
E-mail address: Sebastien.Le.Maistre@jpl.nasa.gov (S. Le Maistre).

http://dx.doi.org/10.1016/j.pss.2016.03.006
0032-0633/

precession to return to the normalized polar moment of inertia, C/MR^2 (M the mass of Jupiter and R its mean radius). Other studies about the estimation of Jupiter's moment of inertia with Juno were mainly focused on the measurement of the Lense–Thirring acceleration (Iorio, 2010; Finocchiaro et al., 2011; Iess et al., 2013; Tommei et al., 2015). This relativistic acceleration of the spacecraft appeared first to be a promising way to constrain Jupiter internal structure and has been predicted by some of these authors to allow estimating C with a relative accuracy of about 2%. However, this precision is one order of magnitude too large to bring significant constraint on Jupiter's core properties as pointed out by Helled et al. (2011).

It is worthwhile to mention that the previous simulations published on Juno's gravity experiment have all been performed assuming an 11-day orbit tracked during one Earth-year. Our simulations are the first ones based on the very recently adopted 14-day orbit over the extended 1.6 Earth-year nominal mission duration.

A brief review of the model-predicted moment of inertia of Jupiter is presented in Section 2. A discussion on the precessional equations of the spin-pole of Jupiter leading to our recommended formula is done in Section 3. Section 4 describes the simulations set up and Section 5 provides and discusses the simulations results. The interest of the VLBI data is assessed in Section 6 and Section 7 summarizes the main results of the paper.

2. Jupiter's polar moment of inertia

We know only a little about the interior of the largest planet of our solar system. Is there a core inside Jupiter? What can be its size and its mass? These are remaining secrets that could be revealed by the Juno orbiter through the determination of the moment of inertia of the whole planet, providing thereby key information on the origin and evolution of Jupiter. Although the interior structure and composition of the giant planet remain very uncertain, we know from its mass–radius relation that Jupiter is not made of pure hydrogen and helium but also contains an additional fraction of heavy elements (Guillot and Gautier, 2007). The mass spectrometer aboard the Galileo probe measured the abundance of heavy elements in the troposphere of Jupiter (Wong et al., 2004). However, it is currently impossible to claim if most of the heavy elements have collapsed in the center to form a dense core or if they are still distributed in the envelope. Measuring the MOI related to the density profile inside the planet will help to answer this critical question about Jupiter's interior.

Different methods have been used to predict the MOI of Jupiter. Jeffreys (1924) used the Radau–Darwin approximation to infer the MOI from the second degree gravity coefficient, J_2. The large MOI value they obtained (see Table 1) indicates a small or even non-existent core. However this first order approximation is not unequivocal and the MOI could actually be shifted considering higher order terms of the Radau–Darwin equation. Helled et al. (2011) provided a range of MOI based on a simple core/enveloppe interior model of Jupiter exactly fitting the measured zonals J_2 and J_4 and matching J_6 within its error bar. They found a range of possible MOI centered on 0.2637 and varying by $\pm 0.3\%$ allowing for either a core as large as one third of the planet size, with a mass up to 40 Earth mass, or no core at all. These authors nevertheless acknowledge that the range provided is interior-model-dependent and could be biased. Finally, a more peculiar method has been used by Ward and Canup (2006) to deduce the MOI of Jupiter from its obliquity. These authors assumed that a portion of the obliquity of Jupiter results from a spin-orbit secular resonance with Uranus whose orbital plane precession rate was observed to be close to the Jupiter polar precession rate. The several-percent-smaller value they obtained (see Table 1) would be in favor of a massive core, but is maybe more speculative.

Table 1
Non-exhaustive published values for Jupiter normalized polar moment of inertia.

Reference	C/MR^2	Core properties	Technics
Jeffreys (1924)	0.265	Small or inexistent	Radau–Darwin approximation
Hubbard and Marley (1989)	0.264	Not constraining[a]	Most plausible interior model
Ward and Canup (2006)	0.236	Massive	Dynamical considerations
Helled et al. (2011)	0.2629–0.2645	$M_{core} < 40 M_{Earth}$ $R_{core} < 0.3 R_{Jupiter}$	Core/enveloppe interior model

[a] Helled et al. (2011) hinge value.

In conclusion, the MOI predicted by the theories (geophysical and dynamical) are model-dependent and not in accordance with each other, currently providing only a poor constraint on the interior structure and composition of Jupiter. Therefore trying to determine the actual MOI of Jupiter with Juno is of great interest. If obtained with enough precision (tenth of percent, Helled et al., 2011), such a measurement could definitely prove the existence of a heavy-element core and bring strong constrain on its mass and size taking a huge leap forward in our comprehension of Jupiter, the solar system and beyond (Guillot and Gautier, 2007; Bolton, 2010).

3. Jupiter's pole precession

Due to the gravitational torque from the Sun on the Jovian system, the orientation of the spin-axis of Jupiter changes in inertial space, sliding the equatorial plane of the planet along the invariable plane of the Sun-Jupiter system (slightly inclined from Jupiter orbital plane) by an angle equal to $\dot{\psi}(t-t_0)$ with respect to the pole direction at epoch t_0. This very slow motion of the tilted rotation axis around the invariable plane pole is called precession and is characterized by the rate $\dot{\psi}$ at which the pole orientation evolves. $\dot{\psi}$ is inversely proportional to the planet normalized polar moment of inertia, C/MR^2, giving the precession rate a real geophysical interest. However, returning to the MOI from a precise measurement of $\dot{\psi}$ is not straightforward since the precessional equations are not obvious, especially in the case of a planet with a batch of accompanying satellites as for Jupiter. Indeed, as pointed out by Ward (1975), the presence of its numerous moons (especially the four Galilean satellites) plays a major role in the precessional motion of Jupiter spin pole.

3.1. Proposed precession model

In this section we provide a new precession model for Jupiter. Starting from the equation of rotational motion of the planet's pole torqued by the Sun and k satellites, the basic equations for the long term motion of the right ascension, α, and declination, δ, of Jupiter's pole are Jacobson (2014)

$$\dot{\alpha}\cos\delta = -\frac{3}{2}\left(\frac{MR^2 J_2}{C\dot{\omega}}\right)\left[\frac{\mu_\odot}{r_0^3}\left(\hat{\mathbf{h}}_0\cdot\hat{\mathbf{s}}\right)\left(\hat{\mathbf{h}}_0\cdot\hat{\mathbf{g}}\right)+\sum_{j=1}^{k}\frac{\mu_j}{r_j^3}\left(\hat{\mathbf{h}}_j\cdot\hat{\mathbf{s}}\right)\left(\hat{\mathbf{h}}_j\cdot\hat{\mathbf{g}}\right)\right] \quad (1)$$

$$\dot{\delta} = \frac{3}{2}\left(\frac{MR^2 J_2}{C\dot{\omega}}\right)\left[\frac{\mu_\odot}{r_0^3}\left(\hat{\mathbf{h}}_0\cdot\hat{\mathbf{s}}\right)\left(\hat{\mathbf{h}}_0\cdot\hat{\mathbf{f}}\right) + \sum_{j=1}^{k}\frac{\mu_j}{r_j^3}\left(\hat{\mathbf{h}}_j\cdot\hat{\mathbf{s}}\right)\left(\hat{\mathbf{h}}_j\cdot\hat{\mathbf{f}}\right)\right] \tag{2}$$

where

J_2	Jupiter's second zonal gravity harmonic coefficient
$\dot{\omega}$	Jupiter's rotation rate
C	Jupiter's polar moment of inertia
$\mu_\odot$	*GM* of the Sun
μ_j	*GM* of satellite *j*
r_0	distance of Jupiter from the Sun
r_j	distance of Jupiter from the satellite *j*
$\hat{\mathbf{h}}_0$	the unit vector normal to the Jupiter centered orbit of the Sun
$\hat{\mathbf{h}}_j$	the unit vector normal to the Jupiter centered orbit of satellite *j*
$\hat{\mathbf{s}}$	Jupiter pole vector
$\hat{\mathbf{f}}$	vector along the ICRF node of the Jupiter equator
$\hat{\mathbf{g}}$	vector completing the orthogonal coordinate system

These equations are analogous to those given in Chapter IV of Sampson (1921) for the representation of the motion of Jupiter's equator. Our analytical expressions of the pole rates are

$$\begin{aligned}\dot{\alpha} = \frac{3MR^2 J_2}{4C\dot{\omega}\cos\delta}\sum_{j=0}^{k}\left(\frac{\mu_j}{\mu_0}\right)\frac{n_j^2}{\left(1-e_j^2\right)^{3/2}}\Bigg[&\left(1-\frac{3}{2}\sin^2 I_j\right)\sin 2i_j\cos\Delta_j\\ &+\sin 2I_j\cos^2(i_j/2)\left[1-4\sin^2(i_j/2)\right]\cos(\Omega_j+\Delta_j)\\ &+\sin 2I_j\sin^2(i_j/2)\left[1-4\cos^2(i_j/2)\right]\cos(\Omega_j-\Delta_j)\\ &-2\sin^2 I_j\sin(i_j/2)\cos^3(i_j/2)\cos(2\Omega_j+\Delta_j)\\ &+2\sin^2 I_j\cos(i_j/2)\sin^3(i_j/2)\cos(2\Omega_j-\Delta_j)\Bigg]\end{aligned} \tag{3}$$

$$\begin{aligned}\dot{\delta} = \frac{3MR^2 J_2}{4C\dot{\omega}}\sum_{j=0}^{k}\left(\frac{\mu_j}{\mu_0}\right)\frac{n_j^2}{\left(1-e_j^2\right)^{3/2}}\Bigg[&\left(1-\frac{3}{2}\sin^2 I_j\right)\sin 2i_j\sin\Delta_j\\ &+\sin 2I_j\cos^2(i_j/2)\left[1-4\sin^2(i_j/2)\right]\sin(\Omega_j+\Delta_j)\\ &-\sin 2I_j\sin^2(i_j/2)\left[1-4\cos^2(i_j/2)\right]\sin(\Omega_j-\Delta_j)\\ &-2\sin^2 I_j\sin(i_j/2)\cos^3(i_j/2)\sin(2\Omega_j+\Delta_j)\\ &-2\sin^2 I_j\cos(i_j/2)\sin^3(i_j/2)\sin(2\Omega_j-\Delta_j)\Bigg]\end{aligned} \tag{4}$$

with

μ_0	*GM* of Jupiter
n_0	Jupiter's mean orbital motion
n_j	the mean orbital motion of satellite *j*
e_0	Jupiter's orbital eccentricity
e_j	the orbital eccentricity of satellite *j*
I_0	the inclination of Jupiter's orbit to the invariable plane
I_j	the inclination of the orbit of satellite *j* to its Laplace plane
i_0	the inclination of the invariable plane to Jupiter's equator
i_j	the inclination of the Laplace plane of satellite *j* to the Jupiter equator
Ω_0	the node of Jupiter's orbit on the invariable plane
Ω_j	the node of the orbit of satellite *j* on its Laplace plane
Δ_0	the node of the invariable plane on Jupiter's equator
Δ_j	the node of the Laplace plane of satellite *j* on

The Ω's are measured from the intersection of the invariable/Laplace planes with the Jupiter equator, and the Δ's are measured from the intersection of the Jupiter equator with the ICRF reference plane. Assuming $C/MR^2 = 0.264$ and using the numerical values of Table 2 we obtain the rates:

$$\dot{\alpha} = -0.006554^\circ\ /\text{cy and } \dot{\delta} = +0.002476^\circ\ /\text{cy (cy stands for century)}. \tag{5}$$

Note that we can integrate (3) and (4) to obtain expressions for the orientation angles (see Appendix A).

Assuming that the pole ($\hat{\mathbf{s}}$) is precessing about the normal to the invariable plane ($\hat{\mathbf{w}}_0$) with rate $\dot{\psi}$, i.e.

$$\frac{d}{dt}(\hat{\mathbf{s}}) = \dot{\psi}\left(\hat{\mathbf{w}}_0\cdot\hat{\mathbf{s}}\right)\left(\hat{\mathbf{w}}_0\times\hat{\mathbf{s}}\right) \tag{6}$$

we get

$$\dot{\psi} = -2\left(\frac{\dot{\alpha}\cos\delta\cos\Delta_0 + \dot{\delta}\sin\Delta_0}{\sin 2i_0}\right), \tag{7}$$

which, after substituting from (3) and (4), becomes

$$\dot{\psi} = -\frac{3}{2\sin 2i_0}\frac{MR^2}{C}\frac{J_2}{\dot{\omega}}\sum_{j=0}^{k}\frac{\mu_j}{\mu_0}\frac{n_j^2\left(1-\frac{3}{2}\sin^2 I_j\right)\sin 2i_j}{(1-e_j^2)^{3/2}}\cos(\Delta_0-\Delta_j) + \dot{\psi}_{00}. \tag{8}$$

$j=0$ corresponds to the parameters relative to the primary and $1 \le j \le k$ is for the set of satellites. $R=69911$ km is Jupiter's mean radius.

$\dot{\psi}_{00}$ is a small corrective term coming from the incorporation of small long-period variations due to the precession of Jupiter's orbital plane with respect to the invariable plane. In other words, assuming the node of Jupiter's orbit to the invariable plane (Ω_0) slowly sliding at a rate $\dot{\Omega}_0$ along the invariable plane (i.e. $\Omega_0 = \Omega_{00} + \dot{\Omega}_0 t$, with t being time from epoch and Ω_{00} the node at epoch measured from the intersection of the invariable plane and the Jupiter equator), then periodic terms appear in the orientation angle of the spin pole (see Appendix A) that have so long peri-

Table 2
Jovian system dynamical parameters and orbital elements.

Param.	Jupiter	Io	Europa	Ganymede	Callisto
μ (km^3 s^{-2})	126,686,534.20	5959.92	3202.74	9887.82	7179.30
J_2	$14{,}695.6 \times 10^{-6}$	–	–	–	–
$\dot{\omega}$ (deg/day)	870.5360	–	–	–	–
n (deg/day)	9.1503600×10^{-2}	203.488958	101.374724	50.317607	21.571073
e	0.048459	0.004135	0.009371	0.001404	0.007368
I (deg)	1.304032	0.035709	0.530508	0.234910	0.660810
Ω (deg)	302.659159	133.947277	47.142650	279.100438	171.533370
$\dot{\Omega}$ (deg/y)	0.00201465	−48.504994	−11.919505	−2.612227	−0.623531
i (deg)	2.215940	0.001448	0.016411	0.083281	0.446992
Δ (deg)	159.586765	126.548974	136.948144	140.851829	138.786197

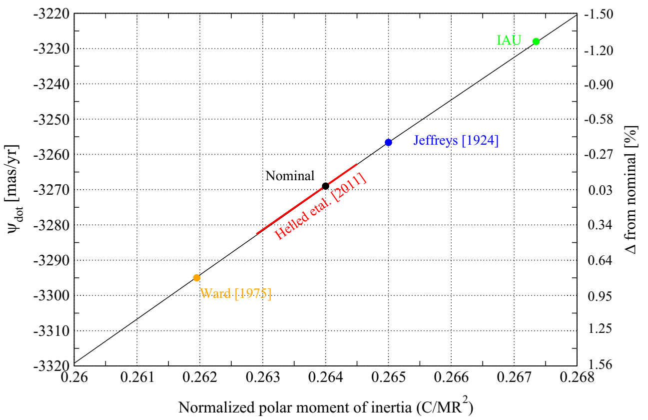

Fig. 1. Jupiter pole axis precession rate as a function of the normalized polar moment of inertia according to Eq. (8). Right y-axis corresponds to the relative difference between the actual precession rate $\dot{\psi}$ reported on left y-axis and the nominal value $\dot{\psi}_n = -3269$ mas/yr.

od ($\dot{\Omega}_0 \simeq 2\times10^{-3}$ deg/y) that one can break them down into constant and rate terms.[1] The latter, denoted here as $\dot{\Psi}_0^{\alpha}$ and $\dot{\Psi}_0^{\delta}$, modify the precession rate of Jupiter pole of rotation according to

$$\dot{\psi}_{00} = -\frac{3}{2\,\sin\,2i_0}\frac{MR^2}{C}\frac{J_2}{\dot{\omega}}\frac{n_0^2}{(1-e_0^2)^{3/2}}(\cos\,\Delta_0\dot{\Psi}_0^{\alpha} + \sin\,\Delta_0\dot{\Psi}_0^{\delta}), \tag{9}$$

where the incorporated rate terms are

$$\begin{aligned}\dot{\Psi}_0^{\alpha} = &+\sin\,2I_0\,\cos^2(i_0/2)[1-4\,\sin^2(i_0/2)]\cos(\Omega_{00}+\Delta_0)\\ &+\sin\,2I_0\,\sin^2(i_0/2)[1-4\,\cos^2(i_0/2)]\cos(\Omega_{00}-\Delta_0)\\ &-2\,\sin^2 I_0\,\sin(i_0/2)\cos^3(i_0/2)]\cos(2\Omega_{00}+\Delta_0)\\ &+2\,\sin^2 I_0\,\cos(i_0/2)\sin^3(i_0/2)]\cos(2\Omega_{00}-\Delta_0),\end{aligned} \tag{10}$$

and

$$\begin{aligned}\dot{\Psi}_0^{\delta} = &+\sin\,2I_0\,\cos^2(i_0/2)[1-4\,\sin^2(i_0/2)]\sin(\Omega_{00}+\Delta_0)\\ &-\sin\,2I_0\,\sin^2(i_0/2)[1-4\,\cos^2(i_0/2)]\sin(\Omega_{00}-\Delta_0)\\ &-2\,\sin^2 I_0\,\sin(i_0/2)\cos^3(i_0/2)]\sin(2\Omega_{00}+\Delta_0)\\ &-2\,\sin^2 I_0\,\cos(i_0/2)\sin^3(i_0/2)]\sin(2\Omega_{00}-\Delta_0).\end{aligned} \tag{11}$$

Applied to the Jovian system (considering here only Jupiter and the four Galilean satellites) with the parameter values taken from Table 2 and with $C/MR^2 = 0.264$, we get from Eq. (8) a predicted value of the nominal precession rate of Jupiter's pole equal to

$$\dot{\psi}_n = -3269 \text{ mas/yr} \tag{12}$$

with a contribution from the precession of its orbital plane equal to

$$\dot{\psi}_{00} = -336 \text{ mas/yr}. \tag{13}$$

Fig. 1 shows how this theoretical value varies given the MOI reported in Table 1 (the extremely low $\dot{\psi} = -3452$ mas/yr corresponding to the MOI proposed by Ward and Canup, 2006, has not been displayed). Evaluating Eq. (7) using the IAU recommended values, $\dot{\alpha} = -0.006499°$/cy and $\dot{\delta} = +0.002413°$/cy (Archinal et al., 2011) leads to $\dot{\psi} = -3228$ mas/yr. This precession rate as well as the one obtained by Ward (1975) (see discussion in Section 3.2) is also displayed in Fig. 1.

Our model (8) allows us to quantify the contribution to $\dot{\psi}$ of the different torques experienced by Jupiter. It predicts that the Galileans satellites are responsible for about 57% of the total precession rate of Jupiter and that 43% is directly induced by the Sun on the oblate tilted planet. Ganymede (30%) and Callisto (20%) are predicted to be responsible for half of the precessional motion of Jupiter's spin axis. Neglecting the precession of Jupiter orbital plane (i.e. $\dot{\psi}_{00} = 0$) induces an error on $\dot{\psi}$ of about 10% by underestimating the direct solar contribution $\dot{\psi}_0$ to only 35% of the total pole precession rate. The precession due to the Sun can be computed according to

$$\dot{\psi}_0 = -\frac{3}{2}\frac{MR^2}{C}\frac{J_2}{\dot{\omega}}\frac{n_0^2}{(1-e_0^2)^{3/2}}\left(1-\frac{3}{2}\sin^2 I_0\right) + \dot{\psi}_{00}. \tag{14}$$

3.2. Historical models

Ward (1975) first proposed an analytical expression for the contribution of natural satellites to the precession rate of the primary:

$$\dot{\psi} = -\frac{3n_0^2}{2\dot{\omega}}\left(\frac{J_2+q}{C/MR^2+l}\right)\cos\,\varepsilon, \tag{15}$$

where $\varepsilon = i_0 + I_0$ is the obliquity of Jupiter, q is the satellites contribution to J_2 and l is the angular momentum of the k satellites system normalized to $MR^2\dot{\omega}$. They read

$$q = \frac{1}{2R^2}\sum_{j=1}^{k}\mu_j(\mu_0 n_j)^{-2/3} \quad \text{and} \quad l = \frac{1}{R^2\dot{\omega}}\sum_{j=1}^{k}\mu_j(\mu_0 n_j)^{-1/3}. \tag{16}$$

The above expression (15) assumes a zero-eccentricity and a zero-inclination of the orbit of Jupiter and its satellites. Based on the knowledge of that time, and assuming $C/MR^2 = 0.25$, Ward (1975) obtained a precessional period for Jupiter corresponding to a rate of $\dot{\psi} = -2880$ mas/yr when accounting for its satellites. This precession rate is 17% slower than what we get with Eq. (8) when we use the same $C/MR^2 = 0.25$. However, these computed rates differ mostly because of the numerical values used by the authors and because of the different approximations made. In order to properly compare the different formula predictions we recompute Eq. (15) with parameter values taken in Table 2 and with $C/MR^2 = 0.264$. This leads to $\dot{\psi} = -3294$ mas/yr, which is this time 0.76% faster than our nominal value. Without accounting for the satellites, Eqs. (8) and (15) both predict $\dot{\psi}_0 = -1058$ mas/yr if the $(1-e_0^2)^{-3/2}$ Jupiter orbit eccentricity factor is applied to Eq. (15) and if $\dot{\psi}_{00}$ is set to 0 in Eq. (8). However, $\dot{\psi}_{00} = -336$ mas/yr is not negligible, meaning that Eq. (15), considering Jupiter's orbital plane fixed in inertial plane, should be less accurate than Eq. (8).

Thirty years later, Boué and Laskar (2006) derived with minimal approximations the precession equations of a planet with a satellite. However, as acknowledged by the authors, their numerical applications only account for the Sun-planet-satellite without accounting for mutual perturbations or accumulated effects of multiple satellites. This explains why summing the contributions to the planet pole precession they computed for the Galileans satellites ($\dot{\psi}_k$) and for the direct Sun contribution ($\dot{\psi}_0$) leads to a very different precession rate than the one we have (12):

$$\dot{\psi} = \dot{\psi}_0\left(1+\sum_k\frac{\dot{\psi}_k-\dot{\psi}_0}{\dot{\psi}_0}\right) = -3705 \text{ mas/yr} \tag{17}$$

with $\dot{\psi}_0 = -1376$ mas/yr. The latter value for the direct Sun contribution is obtained by scaling the -908.216 mas/yr proposed by the authors, who considered Jupiter as an homogeneous sphere (i.e. $C/MR^2 = 0.4$), by 0.4/0.264. Because of the multiple satellite limitation previously evoked, such a large value of the precession rate (17) is disregarded hereafter.

Helled et al. (2011) used a third numerical value for $\dot{\psi}$ equal to 133 mas/yr. This value is 25 times smaller than our predicted value (12) and can be obtained by computing the angle (θ) between the

[1] Note that the pole of rotation also exhibits shorter periodic terms that have to be incorporated in the pole direction modeling to properly deal with incoming true data (see analytic expressions in Appendix A).

spin-pole direction at t_0 and the spin pole direction at $t_1 = t_0 + 1$ year according to

$$\cos\,\theta = \begin{pmatrix} \cos\,\delta_0\,\cos\,\alpha_0 \\ \cos\,\delta_0\,\sin\,\alpha_0 \\ \sin\,\delta_0 \end{pmatrix} \cdot \begin{pmatrix} \cos\,\delta_1\,\cos\,\alpha_1 \\ \cos\,\delta_1\,\sin\,\alpha_1 \\ \sin\,\delta_1 \end{pmatrix}, \tag{18}$$

with $\alpha_1 = \alpha_0 + \dot{\alpha}(t_1 - t_0)$ and $\delta_1 = \delta_0 + \dot{\delta}(t_1 - t_0)$. However, such an assumption does not account for the tilt of the spin pole with respect to the invariable plane (i_0). The latter being small, a slight shift in the pole's direction (θ) translate into a large shift in the longitude direction of the node ($\Delta\psi$), which can be inferred from θ according to

$$\cos(\Delta\psi) = \frac{\cos\,\theta - \cos^2\,i_0}{\sin^2\,i_0}, \tag{19}$$

with $\Delta\psi = \dot{\psi}(t_1 - t_0)$. Using Archinal et al.'s (2011) numerical values for $\alpha_0, \delta_0, \dot{\alpha}, \dot{\delta}$ in Eq. (18) and i_0 from Table 2 in Eq. (19), one gets $\dot{\psi} = -3451$ mas/yr which is more in line with, but still not equal to what we obtained above from Eqs. (7) and (8) (i.e. -3269 mas/yr).

Taken as they are the published values of the precession rate[2] of the Jupiter's pole, one gets a wide range of values for $\dot{\psi}$ (from -2880 to -133 mas/yr), which are not in accordance with our $\dot{\psi}_n = -3269$ mas/yr nominal value. This range shifts and reduces to $[-3294, -3228]$ mas/yr when ignoring the prediction from Boué and Laskar (2006) equations and the prediction derived from Helled et al. (2011) and it further reduces to $\dot{\psi} \in [-3294, -3269]$ mas/yr by neglecting the older IAU value. This corresponds to 1% variation in $\dot{\psi}$, meaning that, even with a infinitely precise estimation of $\dot{\psi}$, C/MR^2 could suffer of biased estimate at the level of 1%.

We have not investigated deeper the reasons of these differences, coming most probably from the approximations made in the analytical developments (e.g. zero eccentricity, zero-inclination hypothesis in Eq. (15)). However, we emphasized here that inferring the C/MR^2 from $\dot{\psi}$ must be performed carefully in order to infer the MOI without any bias and we recommend using Eq. (8) for that purpose, as done here in Section 5.

4. Simulation settings

In this paper we carry out detailed and realistic numerical simulations with the JPL Orbit Determination Program (ODP) to assess the precision with which the precession rate of Jupiter's pole of rotation can be measured by Juno. We use ODP first to simulate two-way[3] Doppler and range data and then to perform a covariance analysis based on them. The simulated data are focused on the well defined characteristics of the Juno mission presented here below and summarized in Table 3.

Juno science operations will be in a very elliptical polar orbit with an orbital period of about 14 days. The spacecraft will orbit Jupiter 36 times before deorbiting into its atmosphere. Perijove numbers 4–36 will be dedicated to science observations among which 80% of the pericenter operations will be devoted to the gravity experiment. The latter consists of a nominal 6 h of Earth based radio tracking of the spacecraft around each of the 26 gravity-pericenter passes. Juno's radio subsystem includes two coherent transponders communicating in X-band (7.2 GHz uplink, 8.4 GHz downlink) and Ka-band (34 GHz uplink, 32.5 GHz downlink), respectively. Since the orbit numbers 4, 6, 7, 8, 9 and 14 will be granted to the Microwave Radiometer (MWR) for probing the deep atmosphere of Jupiter, there will be no Ka-band data then but

Table 3
Juno's gravity experiment characteristics.

Parameter	value
Orbital period	14 days
Mean motion	$n_s = 5.2 \times 10^{-6}$ rad/s
Eccentricity	$e = 0.95$
Inclination	$\hat{i} = 90°$
Semi-major axis	$a = 1{,}670{,}000$ km
Orbital plane	Closer to face-on
Frequency band	Ka-band (32.5 GHz)
Doppler noise	10 μm/s@60 s
Ground tracking station	DSS-25 (34-m at Goldstone)
Nominal tracking duration	~6 h about pericenter
Jupiter orbit insertion (JOI)	July 5, 2016
Nominal mission duration	595 days
Gravity science start	November 11, 2016
Gravity science end	January 23, 2018
Science/gravity operations	32/26 passes

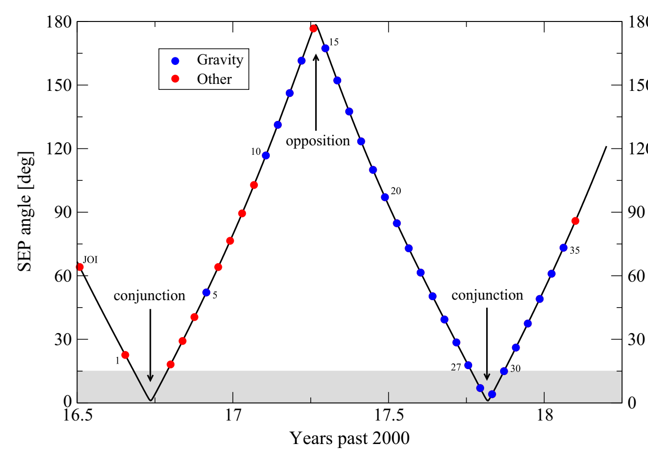

Fig. 2. Sun–Earth-Probe angle during operations. Blue dots locate the tracking time of Juno. The grey area shows the region of very high plasma noise in the raw data. Small numbers reported along the curve are orbit's numbers. (For interpretation of the references to color in this figure caption, the reader is referred to the web version of this paper.)

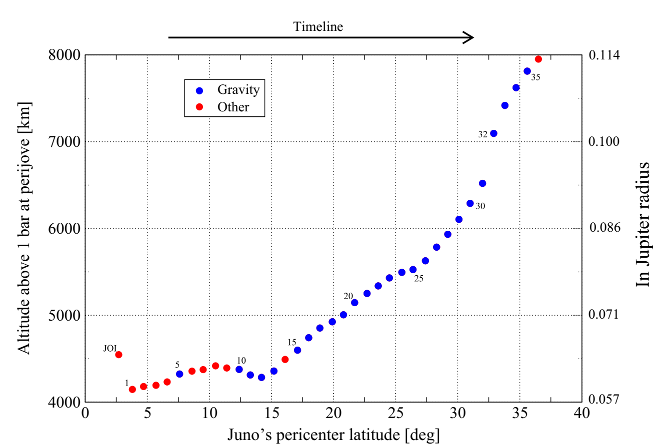

Fig. 3. Juno's pericenter altitude above the 1 bar level versus the pericenter latitude. Passes dedicated to gravity experiment are in blue. Small numbers reported along the curve are orbit's numbers. (For interpretation of the references to color in this figure caption, the reader is referred to the web version of this paper.)

---

[2] We mean here that the numerical values are from the authors. For instance, even if $\dot{\psi}$ does not appear as it is in the papers, the equivalent precession period does, or $\dot{\alpha}$ and $\dot{\delta}$.

[3] Round-trip signal between the spacecraft and a given ground station on Earth.

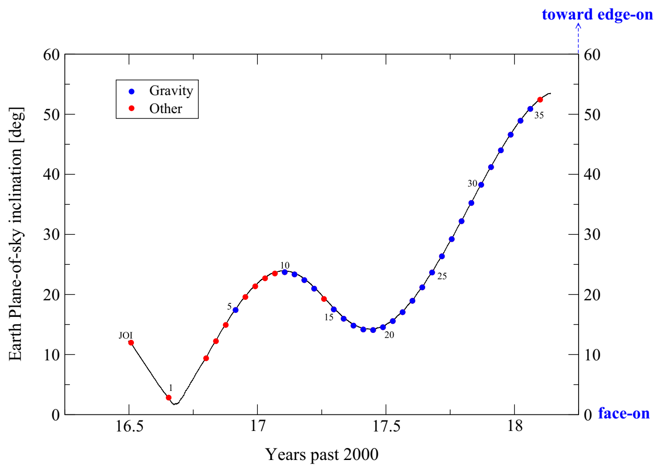

Fig. 4. Orbital plane inclinations of Juno with respect to the Earth plane-of-sky, normal to the Earth-Jupiter direction. Blue dots locate the tracking time of Juno. Small numbers reported along the curve are orbit's numbers. (For interpretation of the references to color in this figure caption, the reader is referred to the web version of this paper.)

the X-up/X-down radio link should be established during the pericenter pass of those orbits. The nominal configuration for the gravity experiment is considered here to be based on the Ka-band data only (blue dots in Figs. 2–4). However, the optimal case consisting to include the X-band data is also tested. Note that the orbit number 1 could also be X-band tracked improving the tracking timespan by 95 days, which could be useful to better determine the precession rate of Jupiter's spin pole.

In real operations both transponders will operate simultaneously during the nominal gravity experiment. Because the charged-particles contribution to Doppler is inversely proportional to the radio signal frequency, the Ka-band data will be poorly degraded by the solar plasma over most of the science phase of the mission when the SEP (Sun–Earth-Probe) angle remains greater than 15°. As shown in Fig. 2, only orbits 27–30, acquired around the solar conjunction, could have significant plasma noise. However, a suitable combination of both X- and Ka-band signals (as it is customarily done using X- and S-band) will enable to cancel most of the plasma noise in the radio-science data to the water vapor noise level, ensuring a very small plasma noise in the Ka-band data over the whole mission.

Only the Deep Space Station (DSS)-25 located at Goldstone in California's Mojave desert will be used to track Juno for gravity science since it is the only NASA station to enable transmitting (uplink) in Ka-band. During the nominal 6 h per orbit of DSS-25 observations, the radio signal will be acquired with an elevation ranging approximately between 10° and 50°, which ensure a small noise contribution from the Earth troposphere. Therefore, the Juno's Ka-band two-way Doppler and range measurements should be of a rather good quality that is why we assume a noise level of 10 μm s^{-1} at 60 s of integration time for the Doppler and of about 2 m for the range. Note that we consider only one range measurement per pass.

As shown in Fig. 3, the pericenter altitude of Juno will increase with time and drift northward in latitude by almost 1° per orbit due to the strong oblateness of Jupiter and the high eccentricity of the orbit. At pericenter, Juno will overfly Jupiter at an altitude ranging between ~4200 km and ~8000 km above the 1 bar level. After each pericenter pass, the spacecraft altitude increases very rapidly making Juno totally insensitive to the high degree harmonic gravity coefficients shortly after the closest approach. In addition to such a limited area of low pass of Juno, the inclination of its orbital plane relative to the plane normal to the Earth-Jupiter direction (or Earth plane-of-sky) remains between 14° and 51° throughout Juno's science operations (see Fig. 4) and below 25° for the first 25 orbits. The view of the orbit from the Earth is then nearly "face-on", which is known to be unfavorable for orbit determination because most of the accelerations undergone by a spacecraft mainly express along-track. Such orbital characteristics have therefore a significant impact on the determination of the gravity field, but

1. this does not prevent accurate determination of the degree-two zonal gravity coefficient that relates the precession rate and the MOI as shown in Section 5, and
2. a face-on configuration is even favorable for observing the signature in the Doppler data of the precessing orbital plane of Juno as discussed in Appendix D.

The simulations presented here follow the multi-arc strategy established by the previous authors for the orbit reconstruction (Finocchiaro et al., 2011; Iess et al., 2013). That is to say, we consider one data arc to be one tracking window, systematically excluding from the arc the spacecraft maneuvers that will be performed few hours after one pericenter pass to target the next perijove's longitude. This strategy has been chosen in order to avoid the dynamical noise induced by the maneuvers. We thus compute the 14-day orbit of Juno from only ~6 h of tracking ($<2\%$ of time). Nevertheless, such a very small amount of tracking time corresponds to a spacecraft true anomaly ranging between $-125°$ and $+125°$. We have then Ka-band radio observations over 70% of the spacecraft true anomaly, including the periapsis, which explains why the orbit can be properly reconstructed.

The exact timing for the Orbit Trim Maneuvers (OTM) should be fixed only a few weeks before the maneuver date but will nominally happen 4 or 6 h after perijove. To correctly align the *s/c*-axis with the Δv direction needed for the OTM, Juno's attitude will be modified losing by the way the Earth pointing of its 2.5-m fixed antenna. The Spin Burn (SB) allowing such a rotation of the spacecraft will typically happen 1.75 h before the OTM, reducing the maximum radio link duration to 2.25 or 4.25 h after perijove (see Fig. B2). Therefore the 6 h of guaranteed tracking per orbit could be slightly shortened or extended with respect to the 3 h tracking past pericenter of the nominal configuration. Moreover, there is still some flexibility in the radio-science operation such that the tracking pass could be more or less centered on the periapsis. We assess here the impact of such tracking window characteristics on the parameter estimate precisions, considering three more tracking windows of 6 h shifted by -30 min, $+30$ min and by $+1$ h from the perfect perijove centered nominal window. We also consider two longer tracking passes of about 7 h and of maximum tracking time. The latter assumes that DSS-25 tracks Juno when the spacecraft is 10° above the horizon, sometimes stopping before this when an early SB has been scheduled. Details on the tracking characteristics are provided in Appendix B.

We carry out a variance/covariance analysis focused on the determination of the precession rate. Nevertheless, the precession rate uncertainty coming from a least square method is estimated together with those of the Jupiter gravity coefficients and others dynamical parameters in order to take into account the possible correlation between all these variables, that could introduce bias in the precession rate estimates and degrade the associated uncertainties. In all, about 350 parameters are estimated. This includes the initial positions and velocities for each arcs (6×26 parameters) plus corrections in the calculations of the forces undergone by Juno due to the solar pressure (one scale factor estimated per arc), due to Jupiter infrared radiation (one scale factor estimated per arc), and due to spacecraft outgassing (one correction per arc). In addition to these local parameters estimated

Table 4
Expected 1-σ uncertainties of the estimated parameters used to infer the MOI of Jupiter obtained from the nominal 6 h of tracking centered on the pericenter of Juno's orbit.

Parameter	Nominal value	A priori constraint	1-σ absolute precision	1-σ relative precision (%)
α_0	268°.05	100°	$1°.015 \times 10^{-4}$	0.00004
δ_0	64°.49	100°	$8°.82 \times 10^{-5}$	0.00014
$\dot{\psi}$	−3269 mas/yr	10^6 mas/yr	1.99 mas/yr	0.06
J_2	0.014736	2×10^{-2}	9.47×10^{-9}	0.00006
LT	1	10^8	7.56×10^{-1}	75.6

for each pericenter pass, we estimate global parameters from the 26 gravity data arcs as the *GM* of Jupiter, and about 110 gravity coefficients including the first 20 zonal harmonic coefficients and the degree-two Love numbers. Only the five first sectorial coefficients are taken into account, whereas the tesseral gravity coefficients of order one and two are included until degree 20 (see Appendix C for justifications about the choice of this maximum degree). Finally, stacking together all the gravity tracking data also allows us to estimate the Lense–Thirring acceleration experienced by Juno[4] as well as the pole orientation of Jupiter at J2000, and of course its precession rate. Note that we chose as a baseline to fix the secular change in the obliquity of Jupiter spin-axis according to rotation theories (e.g. Reasenberg and King, 1979). In the least square regression, we apply a priori constraints on the parameters. Those applied to our parameters of interest are very low and reported in Table 4, the initial position and velocity parameters have all a priori constraint of 1 km and 1 m/s, respectively. Constraints used for the zonal gravity harmonics (see Fig. C2) equal 100 times their expected value (e.g. Kaspi et al., 2010).

Since an error on the orientation of the Earth will show up as an error on the Jupiter's orientation parameters (including the precession rate), we accounted for them in our study by considering an error of about 0.4 mas[5] on each rotation angles orienting the spin-pole of the Earth. These Earth orientation uncertainties are thus included in the uncertainties of estimated parameters through the use of consider analysis (Bierman, 1977). However, as we will see in the next section, the Jupiter's orientation parameter precisions provided by Juno will still be several times larger than the current Earth's orientation errors. The latter have then a negligible impact on the estimate of the precession rate of Jupiter's pole of rotation.

5. Results and discussion

5.1. Focus on the precession rate

In general, the formal errors we obtained for the 350 parameters estimated here are for the main ones in agreement with the estimation already presented in conference by other authors (Finocchiaro et al., 2011; Iess et al., 2013). Therefore, we will not discuss our results on the gravity field and other parameters except than those allowing to estimate the MOI of Jupiter, namely the precession rate ($\dot{\psi}$), the degree-two gravity coefficient (J_2) and the Lense–Thirring (LT) effect. We also provide the obtained precisions for the orientation angle at t_0, i.e. the spin-axis right ascension (α_0) and declination (δ_0) at J2000, since these two parameters, highly correlated with $\dot{\psi}$, see their formal errors

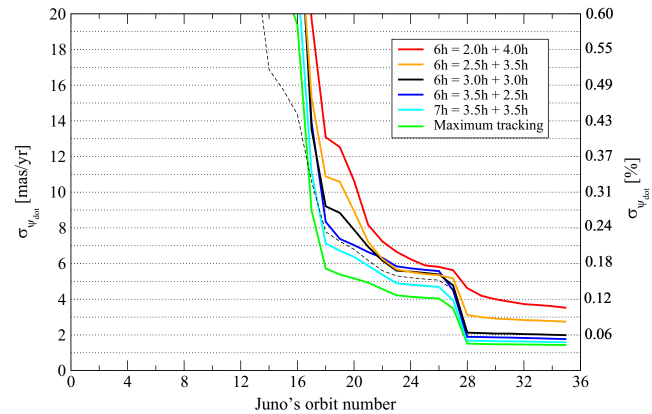

Fig. 5. Time evolution of the 1-σ uncertainties in Jupiter spin axis precession rate as a function of the orbit number of Juno. The expected uncertainties obtained for each of the 6 tracking passes tested in this paper are color-distinguished. Black thin dashed curve has been obtained with 6 h of nominal tracking including X-band pericenter pass numbers 1, 4, 6, 7, 8, 9 for comparison with the nominal black solid curve. (For interpretation of the references to color in this figure caption, the reader is referred to the web version of this paper.)

multiplied by 10 and 8 respectively when estimating the secular change in the orientation of the spin-pole of Jupiter, rather that fixing it as done by most of the previous authors. The other parameters uncertainties are only slightly affected by the precession rate estimation, the largest decrease in precision being on the *GM* of Jupiter, by about 7%, the k_{22} Love number by 3% and the C_{30} gravity coefficient by 1.5%. Although some of the laid aside parameters are reported in Table C1 of Appendix C, we invite the reader to consult the previous study for details.

5.1.1. Nominal tracking scenario

If nominally tracked 3 h before and 3 h after the pericenter pass, the Juno mission will estimate the precession rate of the spin-axis of Jupiter with a precision of about 2 mas/yr. Table 4 reports the predictions obtained on our parameters of interest with such a nominal 6 h of Ka-band radio tracking. The a priori constraints used in the least square fit are also reported in Table 4. They are greatly larger than the post-fit 1-σ uncertainties (by about 6 orders of magnitude), which indicates the strong sensitivity of the Juno's tracking data to our parameters of interest. The time evolution of the nominal 1-σ uncertainty on $\dot{\psi}$ is shown by the solid black curve in Fig. 5. The latter figure also shows, looking at the black dashed curve, how negligible it is to combine the nominal Ka-band data with the X-band measurements that should be obtained at pericenters 1, 4, 6, 7, 8, 9 and 14 in order to better determine the precession rate of Jupiter with Juno. Such a negligible improvement of $\sigma_{\dot{\psi}}$ is due on one hand to the fact that the X-band data acquired at pericenters 1 and 4 close to the solar conjunction (see Fig. 2) are predicted to be respectively 33- and 14-times noisier than the nominal Ka-band data (Folkner, 1994). On the other hand, because the precession signature in the Doppler is mainly controlled by the data time span, in theory, orbits 5 and 35 would be sufficient to measure the secular drift of the spin pole of Jupiter, assuming well known all other forces affecting the spacecraft trajectory. Additional data acquired between these two set of data would thus be theoretically useless to determine $\dot{\psi}$. Obviously the more data points, the more precise are the estimates, but above all, in real life, we critically need as much tracking data as possible to actually determine the best we can the parameters used to model these other forces, otherwise degrading the estimate of the precession rate.

It is worthwhile to mention that including one range data point in each tracking pass is found to have an insignificant contribution

[4] See details on the Lense–Thirring effect in Iorio (2010) for instance.
[5] Deduced from the Earth orientation series provided by the IERS (International Earth Rotation and Reference Systems).

to the precession estimate although useful for Jupiter orbit determination. In addition, also estimating the polar axis secular change in obliquity increases the precession estimate uncertainty by less than a factor of 2.

One time the formal error is relevant: We consider the 1-σ formal error reported in Table 4 as relevant because the data noise statistics of Juno are well known and because we do not expect significant systematic errors since no reaction wheels desaturations nor maneuvers during the tracking are planned. We also ignore the factor of 5 obtained by Folkner (1994) and typically applied to the estimated parameter formal errors from the martian orbiters (Konopliv et al., 2011) to account for the correlations between the measurements due to plasma noise, since the latter should be very small as explained before.

An already better precision than for Mars: The 2 mas/yr of precision obtained by Juno (see Table 4) after about one Earth year of operation is already better than the 6.1 mas/yr of precision obtained by Kuchynka et al. (2014) for the Mars precession rate using about 15 years of abundant radio tracking data from MGS, ODY and MRO. This is first explained by the good quality of the Juno's Ka-band tracking data, with a noise 10 times smaller than the martian X-band data noise. Moreover, due to its very elliptical orbit, Juno's velocity around the perijove is very high ($\sim$55 km/s) compared to that of the quasi-circular martian orbiters ($\sim$3.5 km/s). Therefore, since the Doppler signal is controlled by the spacecraft velocity, the signature of the precession rate will strongly affect Juno's orbit, much more significantly than it affects the Mars orbiters. Finally, as said above, the orbit of Juno is close to face-on during most of the mission (75% of the time with an Earth Plane-of-sky inclination smaller than 30°, see Fig. 4), which is a favorable orbit geometry to measure the precession rate with Doppler data (see Appendix D).

Helled et al.'s (2011) *too small precession rate*: Helled et al. (2011) considered a precession rate equal to 133 mas/yr which is about 25 times lower than the one computed in the present paper. Since the Doppler observable linearly depends on $\dot{\psi}$, the formal errors proposed by the least squares analysis do not depend on the actual value of $\dot{\psi}$. Therefore, the relative accuracy obtained by Helled et al. (2011) can easily be corrected directly scaling their 0.22% prediction by 1/25, obtaining $\sim$0.01% which is (this time) lower than our maximum-tracking best estimate ($\sim$0.04%, see following section). As acknowledged by the authors, their simulation is simple, likely providing too optimistic precision for $\dot{\psi}$. Thus, this can be seen as a threshold, giving us some confidence to our own results, which are a bit worse than 0.01%. It is important to mention here that such a difference between their published value and ours could be crucial to efficiently return to the core properties. Indeed, a precession estimation at 0.22% will poorly reduce the range of core models (see Helled et al., 2011's Fig. 2) whereas an estimate at 0.06%, or better at 0.04%, could really be a key information to distinguish between formation's scenarios.

5.1.2. Other tracking scenarios

Fig. 5 shows the evolution of the precession rate formal error as a function of time for the six tracking coverage described above (including the nominal 6 h-pericentered case). Given such tracking window characteristics, the precession rate will be estimated with a precision ranging between $\sim$0.04% and $\sim$0.11% of its nominal value. Indeed, for such a tracking repartition (centered or not around the periapsis) and duration (in a range of 6 h to about 8 h in average per pass), the precision in the determination of the parameters can be increased or decreased by almost a factor of 2 as shown in Fig. 5. The longer the tracking duration just before the pericenter, the better the precession rate estimate precision and the longer the tracking duration just after the pericenter, the worst. This influence of the tracking coverage dissymmetry with respect to the pericenter is even more significant for the precession parameter determination than the tracking duration itself (Fig. 5). These conclusions are also true for the J2000 spin-pole orientation parameters (α_0, δ_0) but are not necessarily true (or in a minor extent) for the other estimated parameters (see Fig. C1 in Appendix C). Such a better supply on the precession estimate of the tracking acquired before the pericenter is probably due to a better Doppler geometry before the pericenter than after. We note for instance that the line-of-sight elevation above the horizon of the ground station is in average about 20° lower at the beginning of the tracking pass (i.e. before the pericenter) than it is at the end of the pass, which could have some beneficial influence on the orbit determination of Juno. We think that the differences between the solutions in Fig. 5 are also due to the fact that the worst case 6 h=2 h+4 h (red in figures) acquires less Doppler data than the best 6 h-case (3.5 h+2.5 h, blue in figures) at orbits #19 and #20 (see Appendix B) when the spacecraft's orbit is the most sensitive to Jupiter's spin pole precession rate as explained in Appendix D. Although this difference in $\dot{\psi}$ estimate precision due to the tracking schedule is apparently small, it could be crucial in constraining the interior structure of Jupiter as discussed below.

Table 5
Summarize of the current uncertainties in percent in the parameters relating the MOI to the precession rate. Parameters appearing in Eq. (8) not mentioned here are considered as well known. G is the gravitational constant in km^3 s^{-2}.

Parameter	Symbol	Absolute uncertainty	Relative uncertainty (%)
Deg 2 gravity zonal coef.	J_2	0.29×10^{-6}	0.002000
Io's mass	Gm_1	0.012 km^3/s^2	0.000200
Europa's mass	Gm_2	0.009 km^3/s^2	0.000280
Ganymede's mass	Gm_3	0.017 km^3/s^2	0.000170
Callisto's mass	Gm_4	0.013 km^3/s^2	0.000180
Jupiter rotation rate	$\dot{\omega}$	1 s	0.002800
Galileans mean motion	$n_{i=1-4}$	$< 10^{-13}$ rad/s	<0.000001

5.2. Inferring the MOI

In order to infer realistic precision on the geophysical parameter of interest (C/MR^2), one need to account for the lack of knowledge on the different parameters entering in the definition of $\dot{\psi}$ (8), namely $J_2, \dot{\omega}, m_j$ and the orbital parameters of the natural satellites. The mass of Jupiter as well as its orbital characteristics are considered as well known. The uncertainties in J_2 (pre-Juno) and the m_j's are taken from Jacobson's JUP310 solution available on the JPL database (http://ssd.jpl.nasa.gov) and reported in Table 5. As one can find in the literature (e.g. Riddle and Warwick, 1976; Yu and Russell, 2009), the rotation period of jupiter ($\sim$9 h 55 m 29.7 s) is known with an accuracy better than one second. Then, we nominally consider here an uncertainty of 1 s corresponding to about 0.0028% of error on $\dot{\omega}$. Finally, by computing the differences between the last two Jupiter's satellite ephemeris (JUP230 and JUP310), we see that the most significant error in the orbital parameters of the natural satellites affects the Galileans mean motions. These differences are plotted in Fig. 6, where one can see that these largest differences between Jacobson's solutions JUP230 and JUP310 are actually very small, corresponding to a relative accuracy of less than 10^{-6}% of the satellite mean motion, negligibly affecting the inferred MOI precision. Fig. 7 shows the MOI relative precision inferred from the precession estimate precision

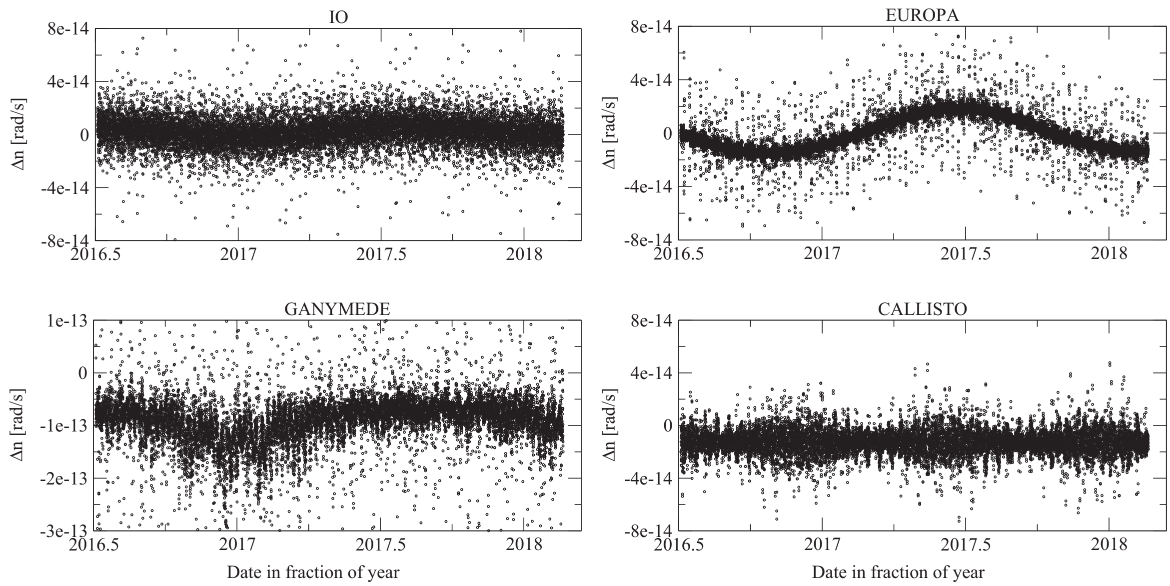

Fig. 6. Differences in Galileans satellite mean motions between JUP230 and JUP310 ($\Delta n = n_{JUP310} - n_{JUP230}$).

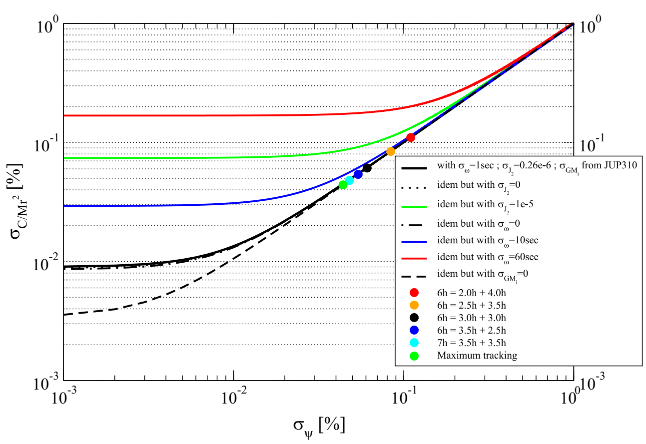

Fig. 7. Jupiter's polar MOI relative precision inferred from the estimation of its pole precession rate. Dots locate the precisions that will be provided by the Juno mission, depending on the tracking characteristics. (For interpretation of the references to color in this figure caption, the reader is referred to the web version of this paper.)

reached after 438 days of Juno gravity operation (see Table 3). Each of the six estimates are plotted (colored dots) along the black solid curve, which considers the above reasonable uncertainties on J_2, $\dot{\omega}$ and the m_j's. As the relative errors of the latter parameters are at least one order of magnitude smaller than our best relative precision for $\dot{\psi}$ (see Table 5), there is no significant contributions of these parameters to the C/MR^2 uncertainties provided by Juno. Therefore, σ_{C/MR^2} should be similar to $\sigma_{\dot{\psi}}$, also ranging between $\sim$0.04% and $\sim$0.11%. The contribution of the J_2, $\dot{\omega}$ and the m_j's "reasonable" uncertainties listed in Table 5 are displayed in Fig. 7 and correspond to the dotted, dashed-dotted and dashed black curves, respectively.

Differential rotation in Jupiter: Jupiter exhibits various zones of different rotation at its surface. We do not know yet how deep the winds of each zone sink into Jupiter's atmosphere. Kaspi (2013) showed that the zonals gravity coefficients will be shifted from those of the Jupiter solid-body at a level depending on the actual depth of these zonal winds. These authors showed in particular that J_2 could be modified by up to 10^{-5}, which is much higher than the 10^{-8} precision we will get on J_2 with Juno (see Table 4). Therefore, besides the fact that Juno may detect the zonal winds contribution in the gravity signal and use it to constrain the depth of the winds (scope of a future paper), the differential rotation in Jupiter if neglected could introduce error in J_2 at the 10^{-5} level. The green solid curve in Fig. 7 shows how such a high level of uncertainty on J_2 would deteriorate the MOI determination, limiting its precision to $\geq 0.08\%$. Nevertheless, this has to be considered as a case study because such a bias on J_2 is very unlikely since its determination from the radio-science data does not depend on the wind models (only its interpretation does). On the contrary, the rotation rate $\dot{\omega}$ is considered as a non-estimated constant when we infer C/MR^2 from the precession rate using Eq. (8). Its value could therefore suffer of bias. Actually, we do not have a good idea of the uncertainty in $\dot{\omega}$ due to deep winds, and the Jupiter that rotates differentially with significant mass involved in the different rotation zones may have a significantly different rotation rate than the basic rotation rate of a solid Jupiter. Therefore, the uncertainty $\sigma_{\dot{\omega}}$ could be large and noticeably affect the MOI estimate precision. The blue and red curves in Fig. 7 show the consequences of an uncertainty on the rotation rate of Jupiter equal to 10 s and 60 s, respectively. If the former ($\sigma_{\dot{\omega}} = 10$ s) does not affect much the precision with which one will get the MOI from the precession rate estimated by Juno, the latter ($\sigma_{\dot{\omega}} = 60$ s) would definitely preclude a precise-enough determination of C/MR^2 in order to significantly constrain the interior structure of Jupiter. Actually, a 10 s of uncertainty on $\dot{\omega}$ appears to be an upper limit beyond what the rotation rate would become the parameter limiting the precise determination of Jupiter's MOI.

Lense–Thirring effect and MOI : As pointed out by several authors, Juno should undergo a significant relativistic acceleration, first predicted in 1918 by Lense and Thirring (see Mashhoon et al., 1984), due to its pericenter high velocity and due to the fast rotation rate of Jupiter. The amplitude of this acceleration is directly proportional to C/MR^2 and has been evaluated by Iorio (2010) to be responsible of a shift of the ascending node of Juno's orbit of about 570 m over one Earth-year. This corresponds to a "gravito-magnetic" precession rate of the orbital node of Juno of 68.5 mas/yr being about 50 times slower than the pole precession rate. As one can expect, such a measurable effect allows us to retrieve the MOI with a relative precision not better than 2–3%, i.e. also about 50 times worse than the precision obtained from the precession rate determination. In fact, such a precision is even optimistic: the theoretical 2–3% is obtainable only by excluding from the fit the angle α_0, since the effects of LT and α_0 are hard to separate with no further information on these two parameters. However, the estimation of the pole angle is necessary to properly wedge the gravity field in space. The actual precision on the MOI inferred from the Lense–Thirring will not be better than 75% in reality (see Table 4).

5.3. Implication for the interior and origin scenarios

Helled et al. (2011) conclude that an MOI estimate with a precision of a few tenths of percent could constrain the internal structure models of Jupiter, even if the constraints will be more or less powerful given what will be the actual value of the MOI. We predict here a precision likely at the level of a few hundredth of percent and definitely better than the 0.22% obtained by Helled et al. (2011). In the worse case we should be able to conclude about the existence of the core (unless the MOI turn out to equal 0.264, Helled et al., 2011), to distinguish between the different model-dependent MOI predictions, supporting some models and excluding others, and we could possibly provide some valuable constraints on the core properties. In the best case, the size and the mass of the core will likely be determined with enough precision to help distinguishing among competing scenarios for the planet's origin.

As summarized in the review of Helled et al. (2014), there are two main scenarios for Jupiter's formation. The giant planet could have been formed first accreting a large and dense core, which would have been then surrounded by a hydrogen–helium envelope, or Jupiter may have formed from gravity instability in the solar primitive nebula so rapidly that possibly no core at all would have time to collapse in the center. In fact there is a collection of hybrid scenarios between these “core accretion model” and “Disk instability model”, and even those two models could end up into a wide range of possible interior structure for Jupiter. They could even have occurred one after the other. It seems therefore that even an exact estimate of the core properties would not ensure the discrimination between the formation models of Jupiter, except for a coreless planet (obviously against the core accretion model). However, if it is not straightforward to return to the exact formation process from a good knowledge of the core properties, it is easy to agree that the formation models of Jupiter will have to account for the heavy-element core mass and size once they will be determined. Generally speaking, once tighter constraints on the heavy-element mass in Jupiter will be obtained from Juno's measurements, formation models of Jupiter will be better constrained (e.g. Helled and Lunine, 2014). This might have strong consequences on the origin and evolution of the entire solar system since Jupiter, as the largest of its inhabitant, undoubtably play(ed) a major role in its evolution.

6. About additional VLBI data

Nowadays, the main techniques used to compute spacecraft trajectories on or around solar system bodies imply ranging and Doppler data exactly as done in the first part of this paper. Those data provide precise information on the distance and radial velocity of the probe with respect to the Earth ground station (i.e. along the line of sight (LOS) direction). The ability of Very Long Baseline Interferometry (VLBI) techniques is to determine the spacecraft position in the plane-of-sky during its flight (i.e. perpendicular to the LOS direction) (e.g. Jones et al., 2011; Duev et al., 2012). Thus, including such data will theoretically provide complementary positional information that could be critical in some cases in determining the precise location of the spacecraft. As previously evoked, during its one Earth year of mission the orbit of Juno will remain almost face-on, offering thus a poor Doppler sensitivity to its orbital motion. Therefore, consider using VLBI tracking data makes sense and one could expect to improve the accuracy of the Juno's reconstructed orbit, allowing for a better detection of the smallest accelerations experienced by the probe such as those induced by the precession rate of Jupiter.

In order to assess the usefulness of adding such data, we make additional simulations with ODP, combining the previously created Doppler and range data with the VLBI data. Actually, we used herein an advanced version of the VLBI data which is called ΔDOR (delta-differential one-way ranging). This data type consists in the difference between measured and nominal two-station time delay differences. In other words, it is the residuals between measured and model predicted difference in the radio signal propagation time between the target and (at least) two Earth based radio-telescopes. The target is alternatively an angularly nearby quasar and the spacecraft itself, moving from one to the other every 5 min along the pass (see details in Curkendall and Border, 2013). Typically, these data provide the spacecraft angular position relative to the quasar in the plane of sky with a precision currently of the order of 1 nrad (i.e. about 0.2 mas). The corresponding ΔDOR measurement noise taken in our simulations equal to 0.025 ns. ΔDOR data are computed here using the 10 radio-telescopes of the Very Long Baseline Array (VLBA), spanning more than 8000 km in the northern hemisphere, between Hawaii and the Virgin islands. These data are created considering for each record the baselines linking the Owens Valley station (closest station to DSS-25 Goldstone station used for Doppler tracking) and the other 9 VLBA stations. ΔDOR data are acquired simultaneously with Doppler data, consisting therefore in a set of 25 passes of about 6 h of 5-min sampled data every 11 days, when Juno is at its periapsis.

We estimate the same parameters that we did before using the Doppler and range data. However, because of the VLBI inherent necessity to track with multiple ground stations in the same time, one has to account for the difference between the stations' clocks. This particular source of error requires estimating additional clock parameters for 9 of the 10 stations, the 10th one providing the reference clock. We model the station time (T_{sta}) error with respect to the reference time (T_{ref}) as follows:

$$T_{ref} - T_{sta} = a + bt + ct^2, \tag{20}$$

with t being the time past the beginning of the tracking pass. The three clock parameters (a, b, c) are estimated for each station and for each tracking pass, leading to $3 \times 9 \times 25$ additional parameters.

Our study revealed that combining such VLBI and Doppler data does not improve the precision we get on any parameter. Typically, VLBI data provide estimates 4–5 orders of magnitude less precise than Doppler data (see Table C1 in Appendix C). For the particular case of the precession rate determination, a similar precision than provided by Doppler could be reached if the accuracy of the interferometric techniques was of the order of 10^{-6} ns.

7. Conclusion

Because of its huge gravitational attraction, Jupiter played the primary role in the formation and evolution of our solar system. The interior structure and composition are fundamental clues to trace back the origin of the largest gaseous planet. They are therefore essential to be known to understand our Solar System as well as other extrasolar systems where giant planets are found in abundance.

We have shown in this paper that the best way to precisely constrain the moment of inertia of Jupiter from Juno is to determine its spin-axis precession rate. We found that the latter allows for a MOI estimate at least 50 times more precise than inferring it from the Lense–Thirring effect as proposed by previous studies. A new precessional equation for Jupiter is also provided and recommended to be used in order to infer the MOI with limited bias.

In addition, we showed that, given the actual tracking repartition and duration that will be performed to compute the orbit of Juno, the precision in the determination of the parameters can be increased (or decreased) by almost a factor of 2 with respect to the 6 h-periapsis-centered nominal tracking estimates. Such a quite small variation can however be critical in order to reach the goal of the mission and could have some consequences on the mission programmatic, depending on what will be the parameters of most interest. It has been found for instance that, given the Doppler geometry offered by the orbital characteristic of Juno, the longer the tracking before the pericenter pass, the more precise is the precession rate estimate. Indeed, the shifting of the tracking pass away from the periapsis-centered nominal configuration by up to one hour is shown to be responsible for a variation in the uncertainty of the pole precession estimate ranging between 0.04% and 0.11% around the nominal $\sigma_{\dot\psi} = 0.06\%$. We found moreover that the MOI will be inferred from the spin-pole precession rate of Jupiter at the same level of relative precision (i.e. $\sigma_{C/MR^2} \in [0.04\%, 0.11\%]$). Therefore, and given the work of Helled et al. (2011), either ($\sigma_{C/MR^2} = 0.11\%$) the MOI determination will "only" allow us to conclude about the existence of the core of Jupiter and sweep some interior- and formation-models away, hopefully providing also some valuable constraints on the core properties, or ($\sigma_{C/MR^2} = 0.04\%$) the core size and mass will likely be determined with enough precision to help distinguish among competing scenarios for the planet's origin.

Finally, we found that VLBI techniques, providing angular position of a spacecraft with an accuracy of 10^{-9} rad in the plane of sky, are totally useless in the precise orbit determination of Juno. These data should be several orders of magnitudes more precise to improve the precision of the geophysical parameter estimations provided by Juno.

Acknowledgments

The research carried out at the Jet Propulsion Laboratory was supported by an appointment to the NASA Post-doctoral Program at the Jet Propulsion Laboratory, administered by Oak Ridge Associated Universities through a contract with NASA. We thank R. Helled for her useful comments.

Appendix A. Analytic expression of Jupiter's pole orientation in right ascension and declination

Assuming that the node of the orbit of body j is $\Omega_j = \Omega_{j0} + \dot\Omega_j t$ with t being time from epoch ($j=0$ corresponds to the parameters relative to the primary and $1 \le j \le k$ is for the set of satellites), we can integrate (3) and (4) to obtain expressions for the orientation angles:

$$\begin{aligned}\alpha = \alpha_0 + \frac{3MR^2J_2}{4C\dot\omega\cos\delta}\sum_{j=0}^{k}\left(\frac{\mu_j}{\mu_0}\right)\frac{n_j^2}{\dot\Omega_j}\left(1-e_j^2\right)^{-3/2}\Bigg[\left(1-\frac{3}{2}\sin^2 I_j\right)\\ (\sin 2i_j \cos\Delta_j)\dot\Omega_j t + \sin 2I_j \cos^2(i_j/2)\left[1-4\sin^2(i_j/2)\right]\sin(\Omega_j\\ +\Delta_j) + \sin 2I_j \sin^2(i_j/2)\left[1-4\cos^2(i_j/2)\right]\sin(\Omega_j-\Delta_j)\\ -\sin^2 I_j \sin(i_j/2)\cos^3(i_j/2)\sin(2\Omega_j+\Delta_j)\\ +\sin^2 I_j \cos(i_j/2)\sin^3(i_j/2)\sin(2\Omega_j-\Delta_j)\Bigg]\end{aligned} \tag{A.1}$$

$$\begin{aligned}\delta = \delta_0 + \frac{3MR^2J_2}{4C\dot\omega}\sum_{j=0}^{k}\left(\frac{\mu_j}{\mu_0}\right)\frac{n_j^2}{\dot\Omega_j}\left(1-e_j^2\right)^{-3/2}\Bigg[\left(1-\frac{3}{2}\sin^2 I_j\right)\\ (\sin 2i_j \sin\Delta_j)\dot\Omega_j t - \sin 2I_j \cos^2(i_j/2)\left[1-4\sin^2(i_j/2)\right]\cos(\Omega_j\\ +\Delta_j) + \sin 2I_j \sin^2(i_j/2)\left[1-4\cos^2(i_j/2)\right]\cos(\Omega_j-\Delta_j)\\ +\sin^2 I_j \sin(i_j/2)\cos^3(i_j/2)\cos(2\Omega_j+\Delta_j)\\ +\sin^2 I_j \cos(i_j/2)\sin^3(i_j/2)\cos(2\Omega_j-\Delta_j)\Bigg]\end{aligned} \tag{A.2}$$

We evaluate the above expressions with the parameter values taken from Table 2 to obtain the terms in the series for the pole angles. Based on these values we find it unnecessary to retain all of the series terms. The reduced series are

$$\begin{aligned}\alpha = \alpha_0 + \frac{3MR^2J_2}{4C\dot\omega\cos\delta}\Bigg\{\sum_{j=0}^{4}\left(\frac{\mu_j}{\mu_0}\right)\frac{n_j^2}{\dot\Omega_j}\left(1-e_j^2\right)^{-3/2}\Bigg[\left(1-\frac{3}{2}\sin^2 I_j\right)\\ (\sin 2i_j\cos\Delta_j)\dot\Omega_j t. + \sin 2I_j\cos^2(i_j/2)\left[1-4\sin^2(i_j/2)\right]\sin(\Omega_j\\ +\Delta_j)\Bigg] + \frac{n_0^2}{\dot\Omega_0}(1-e_0^2)^{-3/2}\Big[\sin 2I_0\sin^2(i_0/2)\left[1-4\cos^2(i_0/2)\right]\\ \sin(\Omega_0-\Delta_0) - \sin^2 I_0\sin(i_0/2)\cos^3(i_0/2)\sin(2\Omega_0+\Delta_0)\Big]\Bigg\}\end{aligned} \tag{A.3}$$

$$\begin{aligned}\delta = \delta_0 + \frac{3MR^2J_2}{4C\dot\omega}\Bigg\{\sum_{j=0}^{4}\left(\frac{\mu_j}{\mu_0}\right)\frac{n_j^2}{\dot\Omega_j}\left(1-e_j^2\right)^{-3/2}\Bigg[\left(1-\frac{3}{2}\sin^2 I_j\right)\\ (\sin 2i_j\sin\Delta_j)\dot\Omega_j t. - \sin 2I_j\cos^2(i_j/2)\left[1-4\sin^2(i_j/2)\right]\cos(\Omega_j\\ +\Delta_j)\Bigg] + \frac{n_0^2}{\dot\Omega_0}(1-e_0^2)^{-3/2}\Big[\sin 2I_0\sin^2(i_0/2)\left[1-4\cos^2(i_0/2)\right]\\ \cos(\Omega_0-\Delta_0) + \sin^2 I_0\sin(i_0/2)\cos^3(i_0/2)\cos(2\Omega_0+\Delta_0)\Big]\Bigg\}\end{aligned} \tag{A.4}$$

Moreover, because the periodic rates for the solar terms are small, we can set

$$\sin(\Omega_0+\Delta_0) = \sin(\Omega_{00}+\Delta_0) + \dot\Omega_0\, t\,\cos(\Omega_{00}+\Delta_0) \tag{A.5}$$

$$\sin(\Omega_0-\Delta_0) = \sin(\Omega_{00}-\Delta_0) + \dot\Omega_0\, t\,\cos(\Omega_{00}-\Delta_0) \tag{A.6}$$

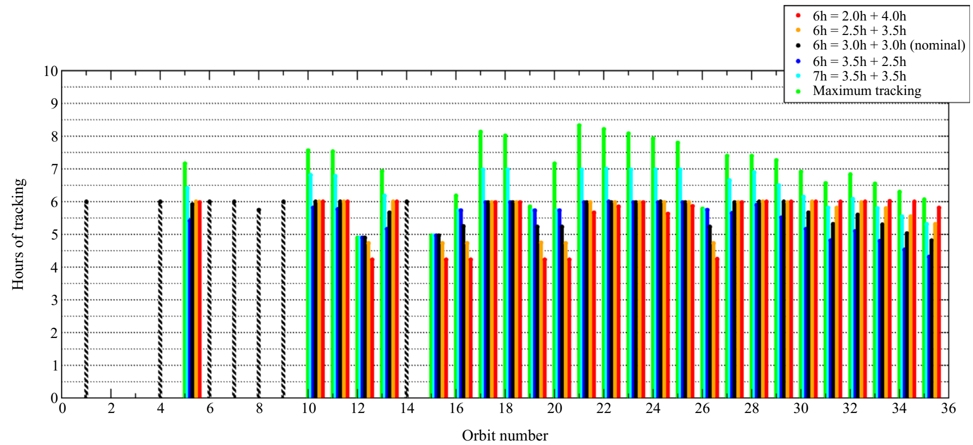

Fig. B1. Ka-band tracking duration per orbit for each of the 6 tracking passes tested in this paper. The black dashed lines are for the X-band simulated data. (For interpretation of the references to color in this figure caption, the reader is referred to the web version of this paper.)

$$\sin(2\Omega_0+\Delta_0) = \sin(2\Omega_{00}+\Delta_0)+2\dot{\Omega}_0\, t\, \cos(2\Omega_{00}+\Delta_0) \quad \text{(A.7)}$$

$$\cos(\Omega_0+\Delta_0) = \cos(\Omega_{00}+\Delta_0)-\dot{\Omega}_0\, t\, \sin(\Omega_{00}+\Delta_0) \quad \text{(A.8)}$$

$$\cos(\Omega_0-\Delta_0) = \cos(\Omega_{00}-\Delta_0)-\dot{\Omega}_0\, t\, \sin(\Omega_{00}-\Delta_0) \quad \text{(A.9)}$$

$$\cos(2\Omega_0+\Delta_0) = \cos(2\Omega_{00}+\Delta_0)-2\dot{\Omega}_0\, t\, \sin(2\Omega_{00}+\Delta_0) \quad \text{(A.10)}$$

and incorporate the “periodic” terms into the constant and rate terms.

Appendix B. Tracking characteristics

We provide in this appendix some characteristics of the 6 tracking configurations considered in this paper:

- Fig. B1 summarizes the tracking duration of the simulated Doppler data used in our simulations. We see on this figure the duration of each pericenter tracking pass for each of the 6 configurations tested in this paper.
- Fig. B2 shows some details of the tracking operations where one can understand for instance what would limit the maximum tracking duration for each arc. Indeed, the first two-way data points that can be measured by DSS-25 correspond to the open green left-pointing triangles tagging the time of reception of a signal transmitted at the minimal 10° of elevation, whereas the last data points would be either marked by the solid green right-pointing triangles, showing when should be performed the SB maneuvers, or by the solid red down-pointing triangles, showing when the signal path moves down to the 10° of elevation threshold.
- Fig. B3 shows the accumulation of Doppler measurements throughout the course of the mission. We note that the worst case 6 h=2 h+4 h (red in figures) acquires less Doppler data during the tracking passes of orbits #19 and #20 than the best 6 h-case (3.5 h+2.5 h, blue in figures), due to early spin-burn maneuvers (see Figs. B2 and B1). However, these two specific orbits correspond to the mission period when Juno is the closest to a face-on orbit configuration (see Fig. 4). This is when the spacecraft's orbit is the most sensitive to Jupiter's spin pole precession rate as explained in Appendix D. In the opposite, the worse-red configuration has more data than the best-6 h-blue configuration after orbit 28, when the plane-of-sky inclination is the greater (i.e. when the orbital plane moves toward an edge-on configuration, see Fig. 4). This ultimately leads to a total number of data for the red scenario similar to the blue scenario (see Fig. B3), but based on datasets less powerful to determine

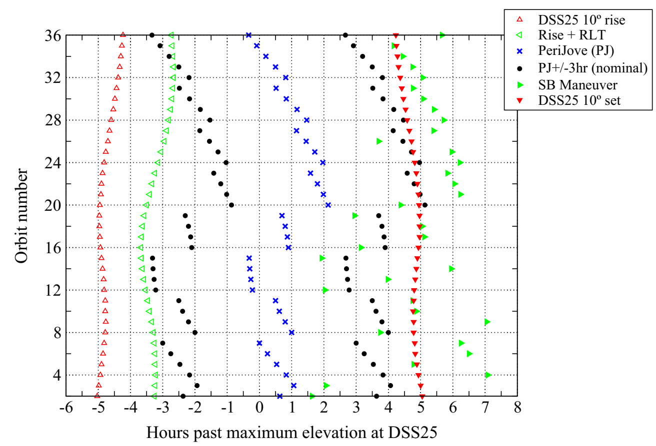

Fig. B2. Radio-signal reception time in hours past the time of maximum elevation during the pass for each orbit. The nominal tracking start and end times are marked with black dots, which corresponds to plus or minus 3 h from the reception of the signal acquired at Juno's pericenter (blue crosses). Red triangles show the maximum period of operation of DSS-25 pointing toward Jupiter when above 10° of elevation. Open green left triangles are obtained by adding the Roundtrip Light Time (RLT) to the time when Jupiter climbs above 10° of elevation. Solid green right triangles correspond to the spacecraft Spin Burn (SB) maneuvers pointing out the end of maximum track when arising before the DSS-25 set time (solid red down triangles). (For interpretation of the references to color in this figure caption, the reader is referred to the web version of this paper.)

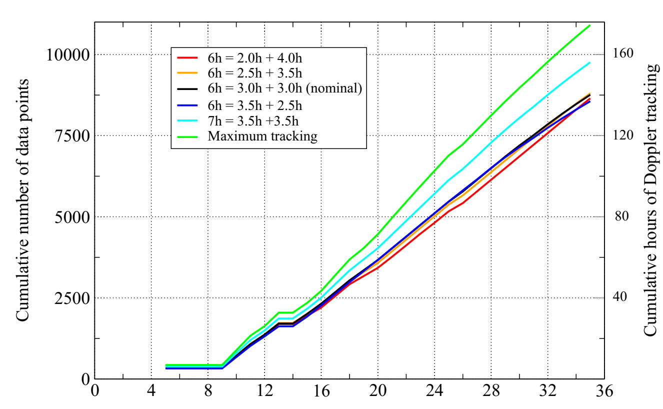

Fig. B3. Cumulative number of data points (left y-axis) and Doppler tracking hours (right y-axis) as a function of the orbit number of Juno. (For interpretation of the references to color in this figure caption, the reader is referred to the web version of this paper.)

the precession rate. These differences in the data acquisition timing might be (partly) responsible for the differences between the precession solution uncertainties in Fig. 5.

Appendix C. Main parameters estimates uncertainties

Together with the precession rate, 350 parameters are estimated from the Juno simulated tracking data. Fig. C1 provides an overview of the changes in the 1-σ formal errors of all these parameters with respect to the nominal 6 h of Ka-band tracking centered on the perijove as a function of the tracking characteristics tested in this paper. The main parameters estimated uncertainties are reported in Table C1 for the nominal scenario, for the worst and best tracking scenarios and for the VLBI stand-alone solutions. Among them, the gravity field zonal coefficients are provided up to degree $n=10$ although zonals are estimated up to $n_{\max}=20$. The latter upper limit has almost no effect on the estimate of the parameters of interest of this paper, but it has significant implication for the zonals estimates themselves as shown in Fig. C2. The deep zonal winds are predicted by Kaspi et al. (2010), Kaspi (2013) to affect the first 8 gravity zonals proportionally less significantly than the higher moments for which the winds contribution could be at the level or even greater than the hydrostatic contribution. From Juno's real data we plan to estimate the first 8 zonals and extract the wind contribution in higher-degrees with another strategy. n_{max} has thus been set in our simulations to 20 since $n_{max} \geq 20$ provide post-fit uncertainties on the first 8 zonals no more depending on n_{max} itself as shown in Fig. C2. The determination of the wind contribution in the gravity

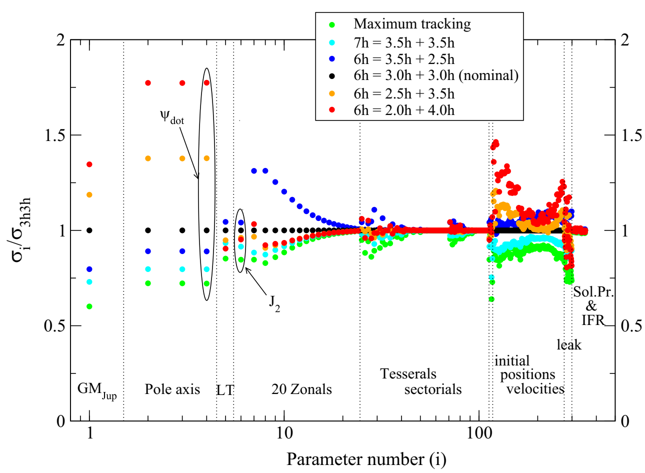

Fig. C1. Impact of the tracking coverage. Ratio between the formal error obtained with a given set of simulated data with respect to the dataset of reference (i.e. with respect to 6 h centered on the pericenter). Colors refer to the same set as in the previous figures. (For interpretation of the references to color in this figure caption, the reader is referred to the web version of this paper.)

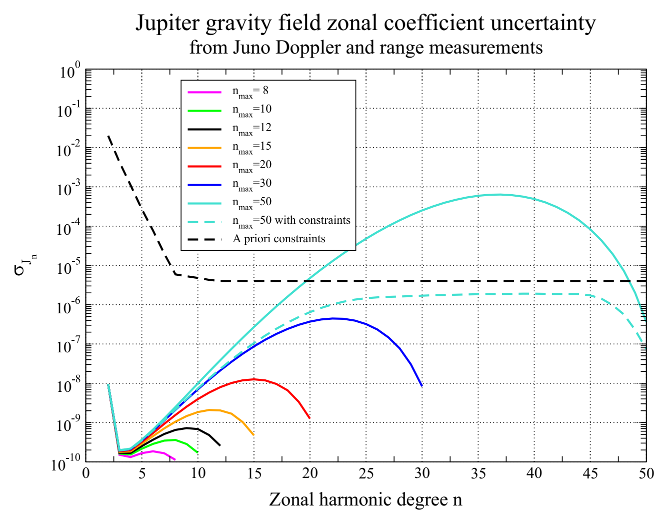

Fig. C2. Jupiter gravity field zonal coefficients uncertainties as a function of n_{max} the degree of the highest zonals estimated.

Table C1
Estimated uncertainties for the main gravity parameters considered in our simulations for three different tracking scenarios (nominal-black, worst-red, best-green) all based on 2-way Ka-band Doppler data at 60 s of integration time. The VLBI stand-alone uncertainties are in last column.

Parameter	Unit	A priori sigma	Doppler 6 h nom.	Doppler 6 h=2 h+4 h	Doppler max. track.	VLBI only 6 h nom.
$GM_{Jupiter}$	km^3/s^2	1.5	1.054e−02	1.419e−02	6.337e−03	1.5[a]
$GM_{Almathea}$	km^3/s^2	1e4	4.668e−02	4.651e−02	2.984e−02	6.1e+02
GM_{Thebe}	km^3/s^2	1e4	4.239e−02	4.535e−02	3.089e−02	6.5e+02
α_0	deg	100	1.028e−04	1.800e−04	7.335e−05	1.2e+00
δ_0	deg	100	8.818e−05	1.563e−04	6.368e−05	1.1e+00
$\dot{\psi}$	deg/cy	100	5.528e−05	9.806e−05	3.986e−05	6.84e−01
LT	%	1e8	76	73	69	⩾100
J_2		2e−2	9.467e−09	9.016e−09	8.013e−09	4.08e−06
J_3		4.3e−3	1.865e−10	1.927e−10	1.579e−10	6.38e−06
J_4		1.1e−3	1.978e−10	1.825e−10	1.639e−10	1.01e−05
J_5		2.7e−4	3.207e−10	2.982e−10	2.756e−10	1.44e−05
J_6		7.7e−5	5.395e−10	5.042e−10	4.773e−10	1.67e−05
J_7		2.0e−5	9.269e−10	8.779e−10	8.425e−10	1.39e−05
J_8		5.9e−6	1.560e−09	1.491e−09	1.447e−09	5.64e−06
J_9		5.3e−6	2.543e−09	2.453e−09	2.398e−09	5.09e−06
J_{10}		4.8e−6	3.951e−09	3.838e−09	3.772e−09	3.97e−06
C_{21}		1.0e−8	1.720e−10	1.824e−10	1.633e−10	[a]
C_{22}		1.0e−8	2.400e−10	2.305e−10	2.117e−10	[a]
S_{21}		1.0e−8	1.827e−10	1.921e−10	1.722e−10	[a]
S_{22}		1.0e−8	3.294e−10	3.155e−10	2.838e−10	[a]
k_{20}		1	1.475e−01	1.402e−01	1.249e−01	[a]
k_{21}		1	7.658e−01	7.866e−01	7.498e−01	[a]
k_{22}		1	2.851e−03	2.871e−03	2.600e−03	[a]

[a] Equal to a priori sigma used.

signal is the subject of a paper in preparation, but ignored in the present paper.

Appendix D. Orbit geometry

As the spin pole of Jupiter precesses, the quasi-fixed orbital plane of the Juno spacecraft in the inertial space will see its orbital inclination changing. This change is slow, corresponding in first approximation to that of angle θ (18), equaling $\dot{\theta} = 133$ mas/yr. For the Jupiter approximated to an homogeneous oblate planet, i.e. only accounting for its strong J_2 in the potential of gravity, only the angular Keplerian elements of Juno will vary with time (Kaula, 1966). Two of them, the mean anomaly ($\hat{M}$) and the argument of perigee ($\hat{\omega}$), are in-orbit variations with small contributions to the Doppler because the orbit is face-on. The third one, the longitude of the ascending node ($\hat{\Omega}$), characterizes an out-of-plane variation of the orbit. The secular changes of these three angles due to J_2 are given by Kaula (1966)

$$\frac{d\hat{M}}{dt} = +\frac{3n_s J_2 R_e^2}{4(1-e^2)^2 a^2}(3\cos^2\hat{i}-1)+n_s, \tag{D.1}$$

$$\frac{d\hat{\omega}}{dt} = +\frac{3n_s J_2 R_e^2}{4(1-e^2)^2 a^2}(5\cos^2\hat{i}-1), \tag{D.2}$$

$$\frac{d\hat{\Omega}}{dt} = -\frac{3n_s J_2 R_e^2}{2(1-e^2)^2 a^2}\cos\hat{i}, \tag{D.3}$$

where $R_e = 71{,}492$ km is the mean equatorial radius of Jupiter, $a, e, \hat{i}$ are the metric Keplerian elements of Juno's orbit and $n_s = 5.2\times 10^{-6}$ rad/s is its mean motion. The precession of the pole of Jupiter leads to $\hat{i} = 90^\circ \pm \varepsilon_{\hat{i}}(t)$, with $\varepsilon_{\hat{i}}(t) \simeq \dot{\theta}\Delta t$ after Δt of orbiting duration. After one Earth year of nominal mission $\varepsilon_{\hat{i}} = 133$ mas, which is still a very small increment in inclination such that $\cos\hat{i} \simeq \varepsilon_{\hat{i}}$ in first order approximation. Since the in-orbit variations (D.1), (D.2) due to the precession of the pole are proportional to $\cos^2\hat{i}$, they are several orders of magnitude smaller than the out-of-plane variation (D.3). In other words, the variations of the ascending node exhibit the largest contribution from the planet's pole precession, making the face-on orbit the most favorable to its determination from Doppler measurements. The expression (D.3) simplifies to

$$\frac{d\hat{\Omega}}{dt} \simeq -\frac{3n_s J_2 R_e^2}{2(1-e^2)^2 a^2}\varepsilon_{\hat{i}}(t) \simeq \varepsilon_{\hat{i}}(t), \tag{D.4}$$

which corresponds to a variation of about $\varepsilon_{\hat{i}} = \theta = 133$ mas after one Earth year. Though small, it corresponds to a perturbation of the velocity of the spacecraft in the normal direction equal to Christodoulidis et al. (1988)

$$\Delta v_n \simeq a\left(1+\frac{e^2}{2}\right)^{1/2}\left[\frac{1}{2}\left(\frac{d\hat{i}}{dt}\right)^2+\left(\frac{d\hat{\Omega}}{dt}\right)^2\sin^2\hat{i}\right]^{1/2}, \tag{D.5}$$

$$\simeq a\left(1+\frac{e^2}{2}\right)^{1/2}\left[\frac{\dot{\theta}^2}{2}+\theta^2\sin^2\hat{i}\right]^{1/2}, \tag{D.6}$$

$$\simeq a\left(1+\frac{e^2}{2}\right)^{1/2}\theta\sin\hat{i} \simeq 42\ \mu\text{m s}^{-1} \tag{D.7}$$

This corresponds to a variation of the radial velocity Δv_r along the signal path ranging between 26.5 μm s^{-1} and 41 μm s^{-1} given the orbit inclination with respect to the Earth plane-of-sky during the mission (Fig. 4). This is above the Doppler measurements noise of Juno (10 μm s^{-1} at 60 s of integration time), suggesting how powerful are such data to determine the precession rate of Jupiter.

References

Archinal, B.A., A'Hearn, M.F., Bowell, E., Conrad, A., Consolmagno, G.J., Courtin, R., Fukushima, T., Hestroffer, D., Hilton, J.L., Krasinsky, G.A., Neumann, G., Oberst, J., Seidelmann, P.K., Stooke, P., Tholen, D.J., Thomas, P.C., Williams, I.P., 2011. Report of the IAU working group on cartographic coordinates and rotational elements: 2009. Celest. Mech. Dyn. Astron. 109 (February), 101–135, http://dx.doi.org/10.1007/s10569-010-9320-4.

Bierman, G.J., 1977. Factorization Methods for Discrete Sequential Estimation. Academic Press, Mineola, New York.

Bolton, S.J., 2010. The Juno mission. In: IAU Symposium, vol. 269, January, pp. 92–100, http://dx.doi.org/10.1017/S1743921310007313.

Boué, G., Laskar, J., 2006. Precession of a planet with a satellite. Icarus 185 (December), 312–330. http://dx.doi.org/10.1016/j.icarus.2006.07.019.

Christodoulidis, D.C., Smith, D.E., Williamson, R.G., Klosko, S.M., 1988. Observed tidal braking in the Earth/Moon/Sun system. J. Geophys. Res. 93 (June), 6216–6236. http://dx.doi.org/10.1029/JB093iB06p06216.

Curkendall, D.W., Border, J., 2013. Delta-DOR: the One-Nanoradian Navigation Measurement System of the Deep Space Network—History, Architecture, and Componentry. JPL Interplanetary Network Progress Report, May.

Duev, D.A., Molera Calvés, G., Pogrebenko, S.V., Gurvits, L.I., Cimó, G., Bocanegra Bahamon, T., 2012. Spacecraft VLBI and Doppler tracking: algorithms and implementation. Astron. Astrophys. 541 (May), A43. http://dx.doi.org/10.1051/0004-6361/201218885.

Finocchiaro, S., Iess, L., Folkner, W.M., Asmar, S., 2011. The determination of Jupiter's angular momentum from the Lense–Thirring precession of the Juno spacecraft. In: AGU Fall Meeting Abstracts, December, p. B1620.

Folkner, W.M., 1994. Effect of uncalibrated charged particles on Doppler tracking. Jet Propulsion Laboratory—Interoffice Memorandum, March.

Guillot, T., Gautier, D., 2007. Giant planets. In: Spohn, T., Schubert, J. (Eds.), Treatise of Geophysics: 'Planets and Moons', vol. 10. Elsevier Publication, Amsterdam, The Netherlands, pp. 439–464, December.

Helled, R., Lunine, J., 2014. Measuring Jupiter's water abundance by Juno: the link between interior and formation models, March. ArXiv e-prints.

Helled, R., Anderson, J.D., Schubert, G., Stevenson, D.J., 2011. Jupiter's moment of inertia: a possible determination by Juno. Icarus 216 (December), 440–448. http://dx.doi.org/10.1016/j.icarus.2011.09.016.

Helled, R., Bodenheimer, P., Podolak, M., Boley, A., Meru, F., Nayakshin, S., Fortney, J.J., Mayer, L., Alibert, Y., Boss, A.P., 2014. Giant planet formation, evolution, and internal structure. Protostars Planets VI, 643–665. http://dx.doi.org/10.2458/azu_uapress_9780816531240-ch028.

Hubbard, W.B., Marley, M.S., 1989. Optimized Jupiter, Saturn, and Uranus interior models. Icarus 78 (March), 102–118. http://dx.doi.org/10.1016/0019-1035(89)90072-9.

Iess, L., Finocchiaro, S., Racioppa, P., 2013. The determination of Jupiter and Saturn gravity fields from radio tracking of the Juno and Cassini spacecraft (Invited). In: AGU Fall Meeting Abstracts, December, p. B1.

Iorio, L., 2010. Juno, the angular momentum of Jupiter and the Lense–Thirring effect. New Astron. 15 (August), 554–560. http://dx.doi.org/10.1016/j.newast.2010.01.004.

Jacobson, R.A., 2014. The orbits of the uranian satellites and rings, the gravity field of the uranian system, and the orientation of the pole of uranus. Astron. J. 148 (November), 76. http://dx.doi.org/10.1088/0004-6256/148/5/76.

Jeffreys, H., 1924. On the internal constitution of Jupiter and Saturn. Mon. Not. R. Astron. Soc. 84 (May), 534.

Jones, D.L., Fomalont, E., Dhawan, V., Romney, J., Folkner, W.M., Lanyi, G., Border, J., Jacobson, R.A., 2011. Very long baseline array astrometric observations of the Cassini spacecraft at Saturn. Astron. J. 141 (February), 29. http://dx.doi.org/10.1088/0004-6256/141/2/29.

Kaspi, Y., 2013. Inferring the depth of the zonal jets on Jupiter and Saturn from odd gravity harmonics. Geophys. Res. Lett. 40 (February), 676–680. http://dx.doi.org/10.1029/2012GL053873.

Kaspi, Y., Hubbard, W.B., Showman, A.P., Flierl, G.R., 2010. Gravitational signature of Jupiter's internal dynamics. Geophys. Res. Lett. 37 (January), L01204. http://dx.doi.org/10.1029/2009GL041385.

Kaula, W.M., 1966. Theory of Satellite Geodesy. Blaisdell Pub. Co., Waltham, MA.

Konopliv, A.S., Asmar, S.W., Folkner, W.M., Karatekin, Ö, Nunes, D.C., Smrekar, S.E., Yoder, C.F., Zuber, M.T., 2011. Mars high resolution gravity fields from MRO, Mars seasonal gravity, and other dynamical parameters. Icarus 211 (January), 401–428. http://dx.doi.org/10.1016/j.icarus.2010.10.004.

Kuchynka, P., Folkner, W.M., Konopliv, A.S., Park, R.S., Le Maistre, S., Dehant, V., 2014. New constraints on Mars rotation determined from radiometric tracking of the opportunity Mars exploration rover. Icarus 229 (February), 340–347. http://dx.doi.org/10.1016/j.icarus.2013.11.015, ISSN 0019-1035, URL ⟨http://www.sciencedirect.com/science/article/pii/S0019103513004879⟩.

Mashhoon, B., Hehl, F.W., Theiss, D.S., 1984. On the gravitational effects of rotating masses: the Thirring–Lense papers. Gen. Relativ. Gravit. 16 (August), 711–750. http://dx.doi.org/10.1007/BF00762913.

Matousek, S., 2007. The Juno new frontiers mission. Acta Astronaut. 61 (November), 932–939. http://dx.doi.org/10.1016/j.actaastro.2006.12.013.

Reasenberg, R.D., King, R.W., 1979. The rotation of Mars. J. Geophys. Res. 84 (October), 6231–6240. http://dx.doi.org/10.1029/JB084iB11p06231.
Riddle, A.C., Warwick, J.W., 1976. Redefinition of system III longitude. Icarus 27 (March), 457–459. http://dx.doi.org/10.1016/0019-1035(76)90025-7.
Sampson, R.A., 1921. Theory of the four great satellites of Jupiter. Mem. R. Astron. Soc. 63, 1.
Tommei, G., Dimare, L., Serra, D., Milani, A., 2015. On the Juno radio science experiment: models, algorithms and sensitivity analysis. Mon. Not. R. Astron. Soc. 446 (January), 3089–3099. http://dx.doi.org/10.1093/mnras/stu2328.
Ward, W.R., 1975. Tidal friction and generalized Cassini's laws in the solar system. Astron. J. 80 (January), 64–70. http://dx.doi.org/10.1086/111714.
Ward, W.R., Canup, R.M., 2006. The obliquity of Jupiter. Astrophys. J. 640 (March), L91–L94. http://dx.doi.org/10.1086/503156.
Wong, M.H., Mahaffy, P.R., Atreya, S.K., Niemann, H.B., Owen, T.C., 2004. Updated Galileo probe mass spectrometer measurements of carbon, oxygen, nitrogen, and sulfur on Jupiter. Icarus 171 (September), 153–170. http://dx.doi.org/10.1016/j.icarus.2004.04.010.
Yu, Z.J., Russell, C.T., 2009. Rotation period of Jupiter from the observation of its magnetic field. Geophys. Res. Lett. 36 (October), L20202. http://dx.doi.org/10.1029/2009GL040094.